Bioorganic Chemistry 91 (2019) 103119

Contents lists available at ScienceDirect

Bioorganic Chemistry

journal homepage: www.elsevier.com/locate/bioorg

Amide-tethered quinoline-resorcinol conjugates as a new class of HSP90 inhibitors suppressing the growth of prostate cancer cells

Kunal Nepali[a,1], Mei-Hsiang Lin[a,1], Min-Wu Chao[b], Sheng-Jhih Peng[a], Kai-Cheng Hsu[b,d], Tony Eight Lin[b], Mei-Chuan Chen[c], Mei-Jung Lai[d], Shiow-Lin Pan[b,d], Jing-Ping Liou[a,c,d,e,*]

[a] School of Pharmacy, College of Pharmacy, Taipei Medical University, Taiwan
[b] The Ph.D. Program for Cancer Biology and Drug Discovery, College of Medical Science and Technology, Taipei Medical University, Taipei, Taiwan
[c] Ph.D. Program in Clinical Drug Development of Herbal Medicine, Taipei Medical University, Taiwan
[d] TMU Biomedical Commercialization Center, Taiwan
[e] School of Pharmacy, National Defense Medical Center, Taipei, Taiwan

ARTICLE INFO

Keywords:
Quinoline
Resorcinol
Chaperone
Cancer
Apoptosis
Heat shock protein

ABSTRACT

The study is focused on the design and synthesis of amide tethered quinoline-resorcinol hybrid constructs as a new class of HSP90 inhibitor. *In-vitro* studies of the synthetic compounds led to the identification of compound **11**, which possesses potent cell growth inhibitory effects against HCT116, Hep3B and PC-3 cell lines, exerted through HSP90 inhibition. Compound **11** triggers degradation of HSP90 client proteins along with concomitant induction of HSP70, demonstrates apoptosis inducing ability and causes G2M phase cell cycle arrest in PC-3 cells. Molecular modeling was used to dock compound **11** into the HSP90 active site and key interactions with the amino acid residues of the HSP90 chaperone protein were determined.

1. Introduction

Heat Shock Protein 90 (HSP90), an ATP dependent molecular chaperone, has been categorized as a crucial facilitator of oncogene addiction and cancer cell survival [1]. A chaperone protein acts as a cellular machine responsible for correct folding and maturation of its client proteins and protects the cellular proteins from degradation by the ubiquitin-proteasome system in conditions of stress [2–7]. HSP90 has been shown to be over-expressed in solid and hematologic tumors which indicates that the continued activity of HSP90 is required for oncogene-driven tumorigenesis. Thus inhibition of the chaperone function of HSP90 may lead to combinatorial targeting of multiple oncogenic protein pathways and thus may overcome the notorious cancer resistance issue [7,8]. Over the years, Hsp90 inhibition has emerged as a fascinating chemotherapeutic strategy for the treatment of diverse malignancies [6,9–11]. The documented activity in this field supports the need to increase the number of investigations on HSP90 inhibitors and this, in turn may escalate the probability of developing cancer therapeutics.

Although HSP90 as a therapeutic target for cancer has been extensively validated using geldanamycin [12–14], the inclination of the medicinal chemist has shifted towards the design of second generation small molecule HSP90 inhibitors (Fig. 1). This could be attributed to limitations such as poor bioavailability and hepatotoxicity that have hampered the clinical growth of ansamycin antibiotics [15]. Resorcinol-based chemical architectures represent a prominent class of second generation HSP90 inhibitors [16–18]. Compounds such as AT-13387 (**4**), STA-9090 (**5**) and NVP-AUY922 (**6**) exemplify HSP90 inhibitors containing a resorcinol moiety [19]. Despite the extensive efforts of the medicinal chemist towards the development of HSP90 inhibitors exerting anti-tumor effects in the last decade, clinical growth of these inhibitors was hampered/limited either by efficacy or adverse events in higher stage trials in addition to pharmaceutical property and commercialization issues [19–22]. As a result, none of the Hsp90 inhibitors are clinically approved yet. The termination of Phase III clinical trials of STA-9090 attributed to acquired resistance exemplifies a case where the clinical advancement of a HSP90 inhibitor was halted by moderate efficacy [19,23]. Overall, it can be concluded that despite the documented promise in preclinical studies and early phase clinical trials, HSP 90 inhibitors have not been able to replicate the effectiveness at higher stage clinical investigations [6,20,24,25]. Experts have indicated that the clinical promise of HSP90 inhibition in cancer is likely to be improved with combination therapies and molecular stratification of patients [26]. However, from the medicinal chemist's perspective, the present scenario in HSP90 inhibitory field makes it quite prudent to

* Corresponding author at: School of Pharmacy, College of Pharmacy, Taipei Medical University, Taiwan.
E-mail address: jpl@tmu.edu.tw (J.-P. Liou).
[1] Contributed equally to this work.

https://doi.org/10.1016/j.bioorg.2019.103119
Received 4 April 2019; Received in revised form 9 July 2019; Accepted 11 July 2019
Available online 15 July 2019
0045-2068/

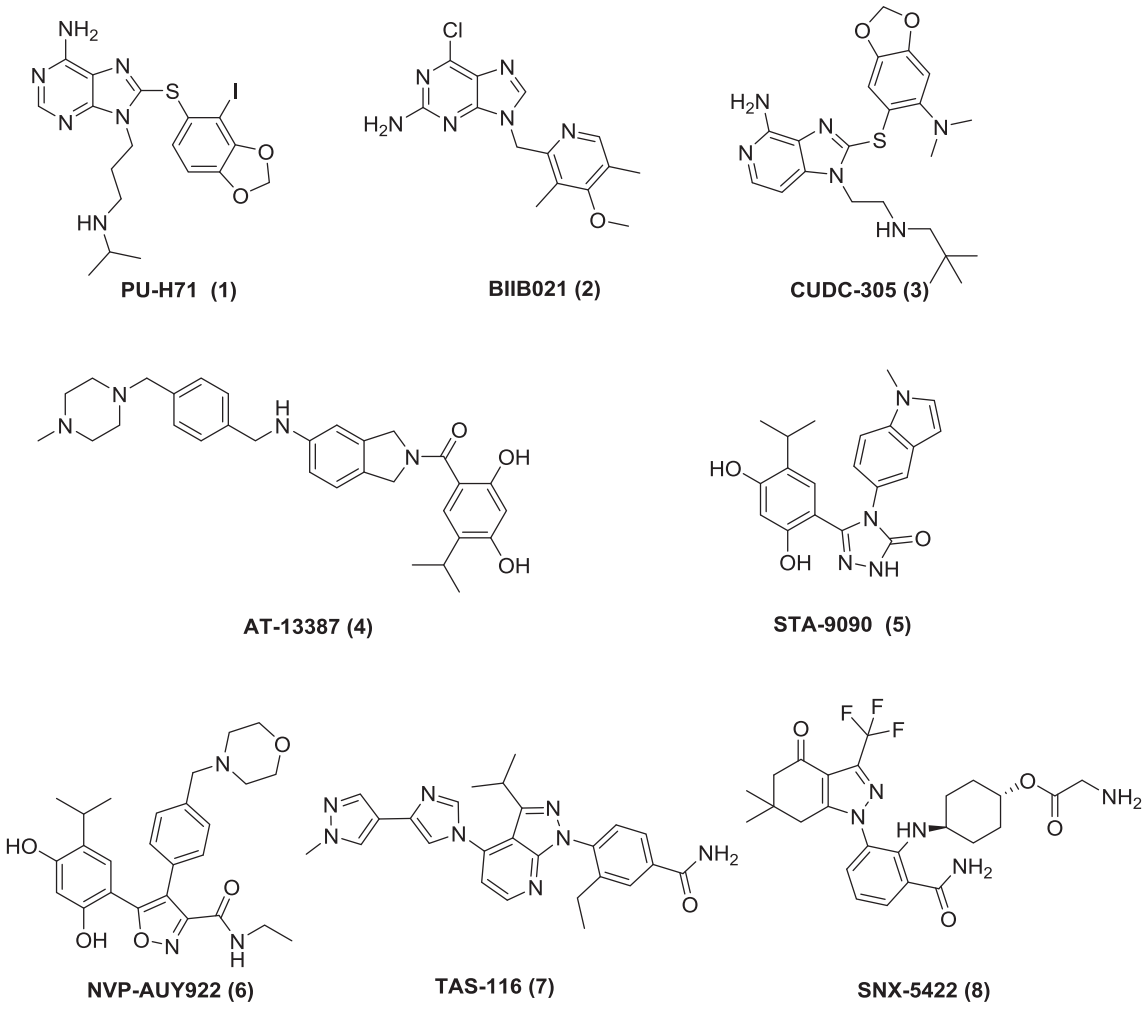

Fig. 1. Chemical structures of HSP90 inhibitors.

expand the pipeline of rationally designed second generation HSP90 inhibitors as new cancer therapeutics. To accomplish this, the design of Hsp90 inhibitors via fusion of existing antitumor pharmacophores furnishing hybrid scaffolds as new chemotypes is anticipated to yield conclusive benefits of HSP90 inhibition in cancer. Other than this, the approach of dual balanced modulation of targets (having a biochemical correlation) may also be able to fully extract the anticancer potential of the chaperone function inhibition. Our ongoing drug discovery program is currently directed towards both these approaches; however this study solely employs the formerly mentioned strategy focused at the design and synthesis of new HSP90 inhibitors.

Identification of key structural motifs and their appropriate fusion has emerged as a rational drug design strategy in recent years [27]. The resorcinol fragment has been recognized as a crucial structural unit present in several second generation HSP90 inhibitors (**4**, **5**, **6**) (Fig. 1). Specifically, the 4-isopropyl resorcinol fragment serves as a key binder associated with the ATP binding site of HSP90 proteins by means of an appropriate fit in the hydrophilic and hydrophobic regions of the protein [20,28,29]. This structural information led us direct our attempts towards the design of resorcinol bearing adducts as Hsp90 inhibitors. The other functionality selected for inclusion in the hybrid structure design was quinoline, a privileged heteroaryl scaffold in cancer drug discovery. The application of this bicyclic heterocycle has been fast spreading in medicinal chemistry owing to its remarkable biological and synthetic versatility [30–32]. Our recent investigations have comprehensively explored quinoline-based anticancer scaffolds which exert antiproliferative effects *via* diverse mechanisms [33–35] and the results of these studies have been extremely optimistic. This indubitably indicates the feasibility along with the ease of inclusion of quinolines as a flexible component in diverse antitumor pharmacophores. Moreover, quinoline-based HSP90 inhibitors have also demonstrated efficacy in some recently conducted studies [31–33]. Based on these revelations, the design of amide bond tethered quinoline-resorcinol hybrids was conceived as a logical strategy in the present study.

Recent medicinal chemistry campaigns of our research group have focused primarily on antitumor constructs bearing bicyclic planar or non-planar/partially hydrogenated (6,6/6,5-fused) heterocycles. In alignment with our ongoing drug discovery program that involves continuous transposition between single target and dual target anticancer chemical architectures, quinoline-resorcinol hybrid constructs as potential Hsp90 inhibitors were designed in the present study (Fig. 2). Employing a fragment linking approach, the designed hybrids were synthesized and their *in-vitro* antiproliferative effects were evaluated. The impact of regio-variations of the fusion, a resorcinol ring on the quinoline core through an amide linkage, along with the influence of alkyl substitution at the amide NH on the cellular activity as well as HSP90 inhibition were also investigated.

2. Results

2.1. Chemistry

The synthetic routes to the target compounds are shown in Schemes 1–3. The quinoline-resorcinol fused constructs (**9**, **13**, **15**, **17** and **20**)

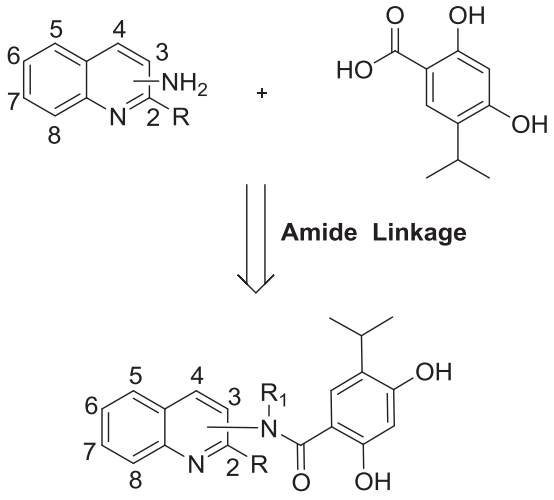

9-22

9: R = H; R_1 = H (3-Position)
10: R = H; R_1 = CH_3 (3-Position)
11: R = H; R_1 = C_2H_5 (3-Position)
12: R = H; R_1 = C_3H_7 (3-Position)
13: R = CH_3; R_1 = H (4-Position)
14: R = CH_3; R_1 = C_2H_5 (4-Position)
15: R = H; R_1 = H (5-Position)
16: R = H; R_1 = CH_3 (5-Position)
17: R = H; R_1 = H (6-Position)
18: R = H; R_1 = CH_3 (6-Position)
19: R = H; R_1 = C_2H_5 (6-Position)
20: R = H; R_1 = H (8-Position)
21: R = H; R_1 = CH_3 (8-Position)
22: R = H; R_1 = C_2H_5 (8-Position)

Fig. 2. Designed hybrids.

were synthesized by a synthetic route depicted in Scheme 1. The quinolines (**23–27**) bearing the amine functional group at different positions were condensed with 2,4-bis(benzyloxy)-5-isopropylbenzoic acid employing amide coupling mediated by EDC/HOBt. The intermediates formed (**28–32**) were debenzylated to yield the final compounds (**9**, **13**, **15**, **17** and **20**). A generalized debenzylation procedure using 10% Pd/C in ethanol in a hydrogenation vessel at 40–42 psi could not be applied to all the intermediates (**28–32)** owing to the tendency of intermediates **29** and **30** to form tetrahydroquinolines. Thus an alternative strategy was followed using Pd/C and formic acid to afford the debenzylated adducts (**13**, **15**).

To further evaluate the effect of *N*-alkylation of the amide NH on the cellular activity as well as HSP90 inhibition, the methods depicted in Schemes 2 and 3 were employed. A similar trend of intermediates responding to different reagents and reaction conditions, generating the target compounds as in Scheme 1 was observed while attempts were made to alkylate the amide NH group. Scheme 2 utilizes cesium carbonate, sodium hydride, potassium *t*-butoxide assisted proton abstraction of the compounds **28**, **31** and **32** to generate the alkylated intermediates (**33–37**). The alkylated intermediates were then subjected to debenzylation with a combination of various reagents and solvents, furnishing the target compounds **10**, **11**, **12**, **19**, and **22**.

While attempting to accomplish the synthesis of the fused constructs **14**, **16**, **18** and **21** through Scheme 2 and employing intermediates (**29**, **30**, **31**, **32**), it was observed that the synthetic methodology could only produce the target compounds in poor yields. The exact reason for the attenuated reactivity with some alkyl iodides and simultaneous formation of degradative products in these cases remains unclear, and a different strategy, shown in Scheme 3 was employed to form the *N*-alkylated target compounds (**14**, **16**, **18**, **21**). The starting materials (**13**, **15**, **17**, **20**) were treated with *tert*-butyldimethylsilyl chloride (TBDMSCl) which led to selective protection of the OH group at the 4′-position. The selective protection of this OH group could be attributed to the hydrogen bonding of the OH at the 2′-position with the carbonyl group of the amide bond. The TBDMS protected intermediates (**38–41**) were then subjected to alkylation using *t*-BuOK (**42–45**) followed by

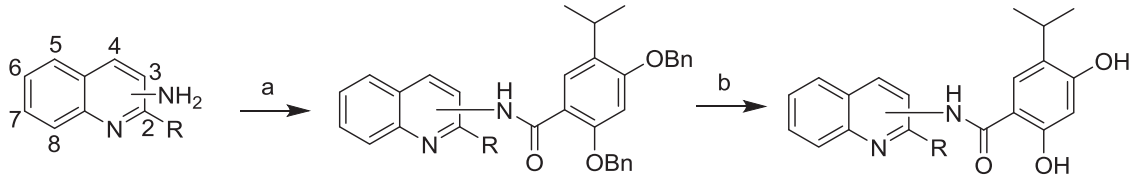

23. R = H, 3-NH_2
24. R = CH_3, 4-NH_2
25. R = H, 5-NH_2
26. R = H, 6-NH_2
27. R = H, 8-NH2

28. R = H (3-Position)
29. R = CH_3 (4-Position)
30. R = H (5-Position)
31. R = H (6-Position)
32. R = H (8-Position)

9 R = H (3 - Position)
13 R = CH_3 (4- Position)
15 R = H (5- Position)
17 R = H (6- Position)
20 R = H (8- Position)

Scheme 1. Reagents and conditions: (a) NMM, EDC, HOBt, DMF, rt; (b) For **9**, **17** and **20**: Pd/C, H_2, EtOH, rt; for **13**, **15**:Pd/C, HCOOH, MeOH, reflux.

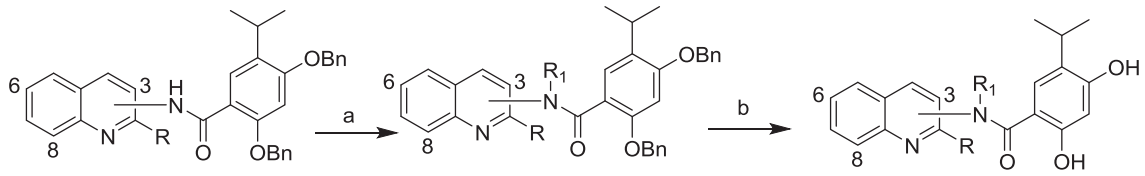

28 R = H (3 - Position)
31 R = H (6- Position)
32 R = H (8- Position)

33 R = H, R_1 = CH_3 (3 - Position)
34 R = H, R_1 = C_2H_5 (3- Position)
35 R = H, R_1 = C_3H_7 (3- Position)
36 R = H, R_1 = C_2H_5 (6- Position)
37 R = H, R_1 = C_2H_5 (8- Position)

10 R = H, R_1 = CH_3 (3 - Position)
11 R = H, R_1 = C_2H_5 (3- Position)
12 R = H, R_1 = C_3H_7 (3- Position)
19 R = H, R_1 = C_2H_5 (6- Position)
22 R = H, R_1 = C_2H_5 (8- Position)

Scheme 2. Reagents and conditions (a) For compound **33**: CH_3I, CS_2CO_3, ACN, rt; for compound **34**: C_2H_5I, NaH, DMF, rt; compound **35–37**: RI, *t*-BuOK, THF, rt; (b) for **10**: Pd/C, H_2, EtOH, rt; for **19**: Pd/C, H_2, MeOH + THF, rt; for **11**, **12** and **22**: Pd/C, HCOOH, MeOH, reflux.

subsequent deprotection of the *tert*-butyldimethylsilyl ethers to furnish the target compounds (**14**, **16**, **18**, **21**).

2.2. Biological evaluation

2.2.1. In-vitro cytotoxicity studies

We systemically investigated the synthetic compounds (**9–22**) for their antiproliferative activity on three human tumor cell lines, HCT116 colorectal cancer cell lines, Hep3B liver cancer cell lines, and PC-3 prostate cancer cell lines. BIIB021, 6-chloro-9-((4-methoxy-3,5-dimethyl-pyridin-2-yl)- methyl)-9H-purin-2-amine (**2**) and 17-AAG were employed as standards. The results presented in Table 1 revealed exciting insights regarding the antiproliferative effects of the synthetic compounds. The compound **11** (*N*-ethyl-2,4-dihydroxy-5-isopropyl-N-(quinolin-3-yl)benzamide) bearing the isopropyl resorcinol functionality tethered *via* an amide bond at position 3 of the quinoline scaffold displayed substantial cytotoxic effects against HCT116, Hep3B and PC-3 cancer cell lines with GI_{50} values of 0.17, 0.33 and 0.14 μM. The adduct **11** is endowed with two-fold higher cell growth inhibitory effects against PC-3 cell lines in comparison to BIIB0201 (**2**) and is equipotent with 17-AAG. Conjugate **11** displays a similar inhibitory profile to that of BIIB021 (**2**) towards the HCT116 cell lines and was

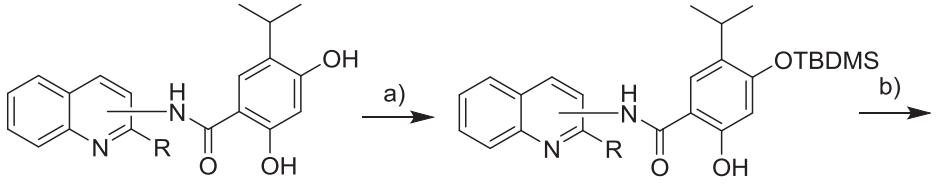

13 R = CH_3 (4- Position)
15 R = H (5- Position)
17 R = H (6- Position)
20 R = H (8- Position)

38 R = CH_3 (4- Position)
39 R = H (5- Position)
40 R = H (6- Position)
41 R = H (8- Position)

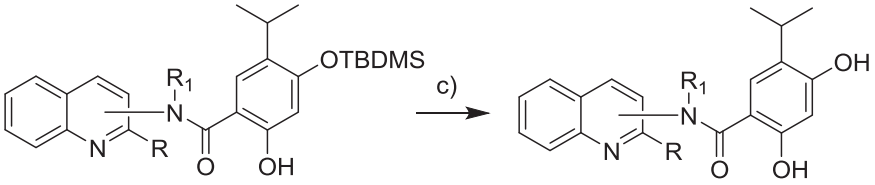

42 R = CH_3, R_1 = C_2H_5 (4-Position)
43 R = H, R_1 = CH_3 (5-Position)
44 R = H, R_1 = CH_3 (6-Position)
45 R = H, R_1 = CH_3 (8-Position)

14 R = CH_3, R_1 = C_2H_5 (4-Position)
16 R = H, R_1 = CH_3 (5-Position)
18 R = H, R_1 = CH_3 (6-Position)
21 R = H, R_1 = CH_3 (8-Position)

Scheme 3. Reagents and conditions (a) TBDMS-Cl, DIPEA, CH_2Cl_2, rt; (b) alkyl iodide, *t*-BuOK, (R_1I), THF, rt; (c) TBAF, CH_2Cl_2, rt.

Table 1
Antiproliferative activity of compounds **9–22** against human cancer cell lines.

Compounds	Cell viability (GI_{50} μM ± SD[a])		
	Prostate PC3	Colorectal HCT116	Liver Hep3B
9	> 10	> 10	> 10
10	> 10	> 10	> 10
11	**0.14 ± 0.01**	**0.17 ± 0.01**	**0.33 ± 0.03**
12	> 10	> 10	> 10
13	> 10	> 10	> 10
14	> 10	ND	ND
15	> 10	> 10	> 10
16	1.81 ± 0.48	> 10	> 10
17	> 10	ND	ND
18	> 10	> 10	> 10
19	0.46 ± 0.13	1.87 ± 0.68	0.69 ± 0.06
20	> 10	> 10	> 10
21	> 10	> 10	> 10
22	2.40 ± 0.27	2.45 ± 0.55	5.19 ± 0.44
BIIB021 (2)	0.28 ± 0.02	0.15 ± 0.02	0.52 ± 0.047
17-AAG	0.14 ± 0.04	0.075 ± 0.007	0.19 ± 0.00

[a] SD: standard deviation, all experiments were independently performed at least three times.

more potent than the standard (**2**) against Hep3B cell lines. A comparative analysis of the cytotoxic profile of the fused construct (**11**) with compounds **9**, **10** and **12** confirmed the favorable activity trend encountered with the *N*-ethylation of the amide NH. Compounds **9** (bearing unsubstituted amide NH), **10** (N-CH_3, amide) and **12** (N-C_3H_7, amide) exhibit relatively diminished activity profiles against the cell lines tested. A decline in the activity profile was seen on translocating the resorcinol fragment from position 3 to 4, 6 and 8 (compare **11** with **14, 19** and **22**). Keeping the *N*-ethyl substitution pattern intact and shifting the site of resorcinol fusion from position 3 to 6 (**19**) retained the cytotoxic effects against the PC-3 (GI_{50} = 0.46 μM), HCT-116 (GI_{50} = 1.87 μM) and Hep3B (GI_{50} = 0.69 μM) cell lines, but the efficacy was less pronounced than that of compound **11**. The 8-quinolinyl substituted compound with an *N*-ethyl substituent (**22**) also demonstrated moderate inhibition of the growth of tumor cell lines. The *in-vitro* cytotoxicity assay clearly indicates that the sites of attachment of the quinoline scaffold and the resorcinol fragment are critical for induction of the antiproliferative effects. Overall, the fusion of the structural motifs at position 3 of the quinoline moiety and *N*-ethyl substitution pattern (amide NH) played a key role in inducing the antiproliferative effects.

Table 2
HSP90 inhibitory activity of compounds **9–22.**

Compounds	IC_{50} ± SD(nM[a]) HSP90α
9	> 10,000
10	> 10,000
11	149.06 ± 0.63
12	196.06 ± 15.88
13	> 10,000
14	> 10,000
15	> 10,000
16	> 10,000
17	> 10,000
18	> 10,000
19	124.22 ± 17.80
20	> 10,000
21	> 10,000
22	172.21 ± 3.74
BIIB021 (2)	132.75 ± 14.75
17-AAG	127.73 ± 17.56

[a] SD: standard deviation, all experiments were independently performed at least three times.

2.2.2. HSP90 inhibition assay

To validate the underlying mechanism of the antiproliferative activity of constructs **9–22**, an *in-vitro* assay was performed and the HSP90 inhibitory potential was evaluated. The data in Table 2 made it evident that only the cytotoxic compounds (**11**, **19**, **22**) are able to modulate the function of the chaperone protein. The compounds unable to induce inhibitory effects against the cell lines tested were also found to be devoid of any activity against HSP90 (IC_{50} > 10000 nM) with the exception compound **12**. Thus the assay results establish a strong dependence of cell growth inhibitory effects of the conjugates on their capacity to inhibit the chaperone protein. Compound **11**, which is endowed with substantial antiproliferative effects, exhibits significant HSP90 inhibitory activity with an IC_{50} value of 149 nM and the results with either of the standards employed were comparable. Compound **22** (quinoline-resorcinol: site of linkage – C8) also inhibited the chaperone activity with IC_{50} = 172 nM. In addition to the activity profile of **11**, the promising cellular and chaperone function inhibitory profile of compound **19** is an important finding (Tables 1 and 2). Compound **19** with IC_{50} = 124 nM was found to be the most potent HSP90 inhibitor. Correlating the results of antiproliferative activity (Table 1) with those from the HSP90 inhibitory assay (Table 2) revealed a similar preference of structural features for HSP90 inhibition as that for cytotoxicity. The *N*-ethyl substitution with positions 3 or 6 as the critical point of attachment of the quinoline scaffold and the resorcinol ring were the favored structural attributes. In light of these assay results, the most potent antiproliferative agent (**11**) with substantial HSP90 inhibitory potential was further investigated to ascertain its HSP90-mediated suppression of prostate cancer cell growth.

2.2.3. Effect of test compounds on HSP90-regulated client proteins

To further establish whether the most potent fused construct (**11**) possesses the signatory features of known HSP90 inhibitors in terms of its capacity to modulate the expression of cellular markers, a western blot analysis was performed. The ability of compound **11** to trigger the downregulation of representative HSP90 client protein expression and induction of HSP70 protein levels was determined in a PC-3 cell line. Western immunoblotting data revealed that **11** induces HSP70 expression and depletes the protein expression levels of client proteins, such as EGFR, AKT, ERK, FAK and Rb indicating selective HSP90 inhibition (Fig. 3A). The underlying mechanism of arrest of PC-3 cells by **11** on the G2/M phase was explored and the expressions of cell cycle related proteins were examined. Induction of p-MPM2 along with cyclin B1 and downregulation of Cdc2 and its phosphorylation of Tyr15 was observed after a 24 h treatment with compound **11** and BIIB021 (**2**) (Fig. 3B). These results suggested that the HSP90 inhibitor (**11**) induces mitotic arrest in prostate cancer cells. Moreover, compound **11** triggers cell apoptosis at 48 h leading to PARP and caspase activations as evident from the levels of cleaved Caspase 3 and PARP (Fig. 3C). The activation of Caspase 3 and PARP is considered to be a hallmark of apoptosis and the results of the western blot analysis clearly indicate the apoptosis inducing ability of **11**. These observations coupled with the results presented in Tables 1 and 2 confirm that mediation of the cell growth inhibitory effects of **11** is a consequence of Hsp90 chaperone inhibition and also confirms the mitotic arrest in prostate cancer cells.

2.2.4. Effects of test compounds on cell cycle distribution

The effect of **11** on the cell cycle progression was evaluated by flow cytometry to validate the underlying mechanism of cell growth repression in PC-3 cells. The results of the experiment indicate that compound **11** and BIIB021 (**2**) cause cell arrest (G2M phase) at 24 h followed by a concentration-dependent apoptotic subG1 accumulation at 48 h (Fig. 4A and B). In addition, it was observed that **11** is more

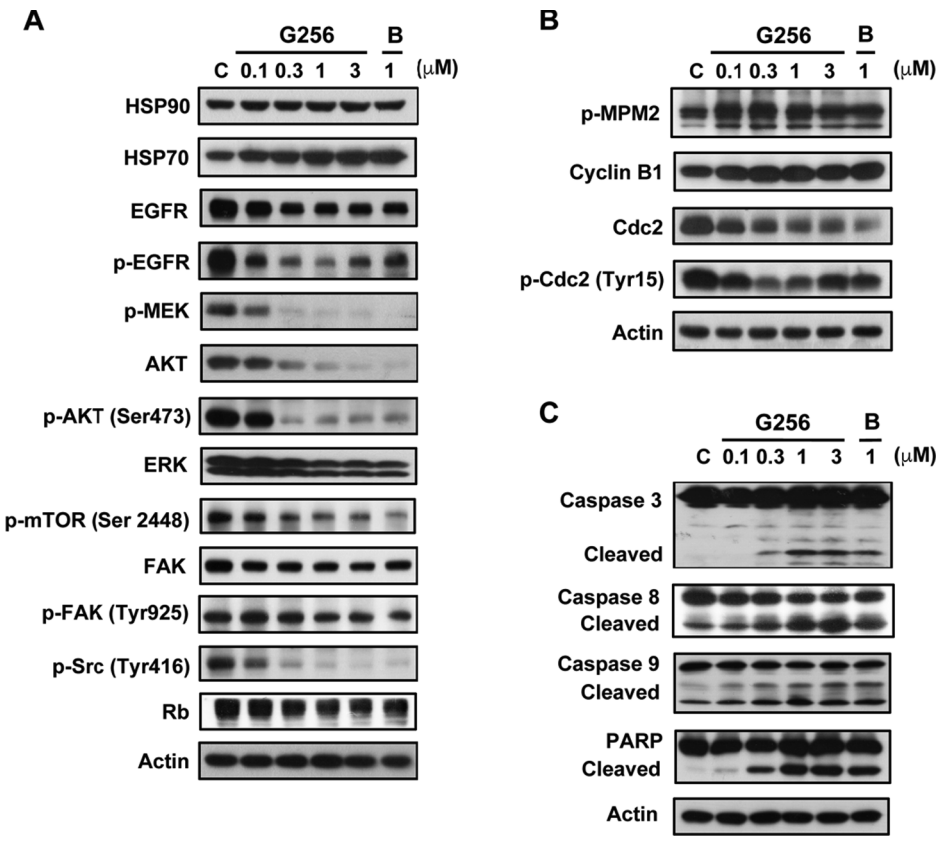

Fig. 3. The effects of **11** on client proteins of HSP90, cell cycle regulated and apoptotic protein levels. PC3 cells were treated with DMSO (Control; C) or 0.03–3 μM of test compounds (**11** or BIIB021) for 24 h. Cells were harvested and subjected to western blot analysis for the detection of various HSP90 client proteins (A) and cell cycle related proteins (B). (C) PC3 cells were incubated with DMSO (Control; C) or 0.03–3 μM of test compounds (**11** or BIIB021) for 48 h to detect the apoptotic proteins. Actin was used as the internal control; B: BIIB021. (**G256** represents **11**).

potent than BIIB021 (**2**) as at 0.3 μM, it causes the initiation of the increase in G2M and subG1 phase population (Fig. 4C and D). These results indicate that the hybrid compound **11** causes dose-dependent G2M arrest and apoptosis in prostate cancer cells.

2.2.5. Molecular modeling studies

A molecular docking study was performed to elucidate the interactions between compound **11** and amino acid residues of the chaperone protein HSP90. Initially, the validation of the docking protocol was performed by redocking the co-crystallized ligand (Fig. 1S. in Supporting Information – SI). This showed that the redocked ligand has a docking pose similar to that of the co-crystallized ligand and indicates that the docking protocol used has a favorable prediction acuity. Compound **11** was then docked into the HSP90 binding site and it was found that it is anchored within the binding site and can be separated into three distinct segments with respect to its HSP90 docking pose (Fig. 5). At Site 1 (S1), the 2,4-dihydroxy-5-isopropylbenzoyl moiety is held in place through hydrophobic interactions with residues Met98, Leu107 and Phe138. In addition, the hydroxyl groups form hydrogen bonds with Asn51 and Asp93, and the carbonyl forms a hydrogen bond with Thr184. At Site 2 (S2), the quinoline moiety of compound **11** occupies a hydrophobic pocket with Ala55 and Tyr61. At Site 3 (S3), the two pharmacophores are connected *via* an *N*-ethyl amide bond. This ethanamine moiety has hydrophobic interactions with Ala55, Ile96, Met98 and Tyr61. In contrast, compounds **9** and **10**, with an unsubstituted amide linkage (–NH-CO–) and an *N*-methyl amide linkage respectively, do not inhibit HSP90 as effectively as **11**, suggesting that the *N*-ethyl substitution is a prerequisite for activity. Together, these interactions shed light on the potency of compound **11** against HSP90.

2.2.6. In vivo antitumor efficacy in human xenografts

Compound **11** was evaluated for its *in vivo* efficacy versus tumor xenografts in nude mice bearing the human PC-3 cancer cell line. PC3-tumor-bearing nude mice were treated with compound **11** (50, 100 and 200 mg/kg/d, by oral gavage qd) and tumor was excised when the tumor size reached 1200 mm^3. It was found that treatment of PC3 xenograft-bearing nude mice with compound **11** resulted in dose dependent decrease of the tumor progression. Construct **11** led to the suppression of tumor growth by a tumor growth inhibition factor (% TGI = 50.1%) without loss of their body weight (Fig. 6). Thus the *in vivo* animal model experiments demonstrated that compound **11** possess moderate *in vivo* potential against prostate cancer.

3. Conclusion

A novel class of inhibitors that potently inhibits HSP90 is reported. By fusing key structural motifs known to induce cell growth inhibitory effects by modulation of the HSP90 chaperone protein, a series of fused quinoline-resorcinol compounds were designed and synthesized. A correlation of the tumor growth inhibition exerted through HSP90 inhibition was established from the results of *in vitro* cytotoxicity studies, HSP90 inhibitory assays and western blot analysis. The site of linkage of the resorcinol ring to the quinoline scaffold *via* an amide bond and *N*-alkylation of amide bond was found to be extremely critical for both the cytotoxicity as well as the modulation of chaperone function. These attempts led us to speculate about the structure activity relationships with ethylation at the amide NH and position 3 (the quinoline ring) as the site of attachment being the structural prerequisites for activity. The main finding of the study is the identification of **11** as an HSP90 inhibitor endowed with apoptosis inducing ability and substantial *in vitro*

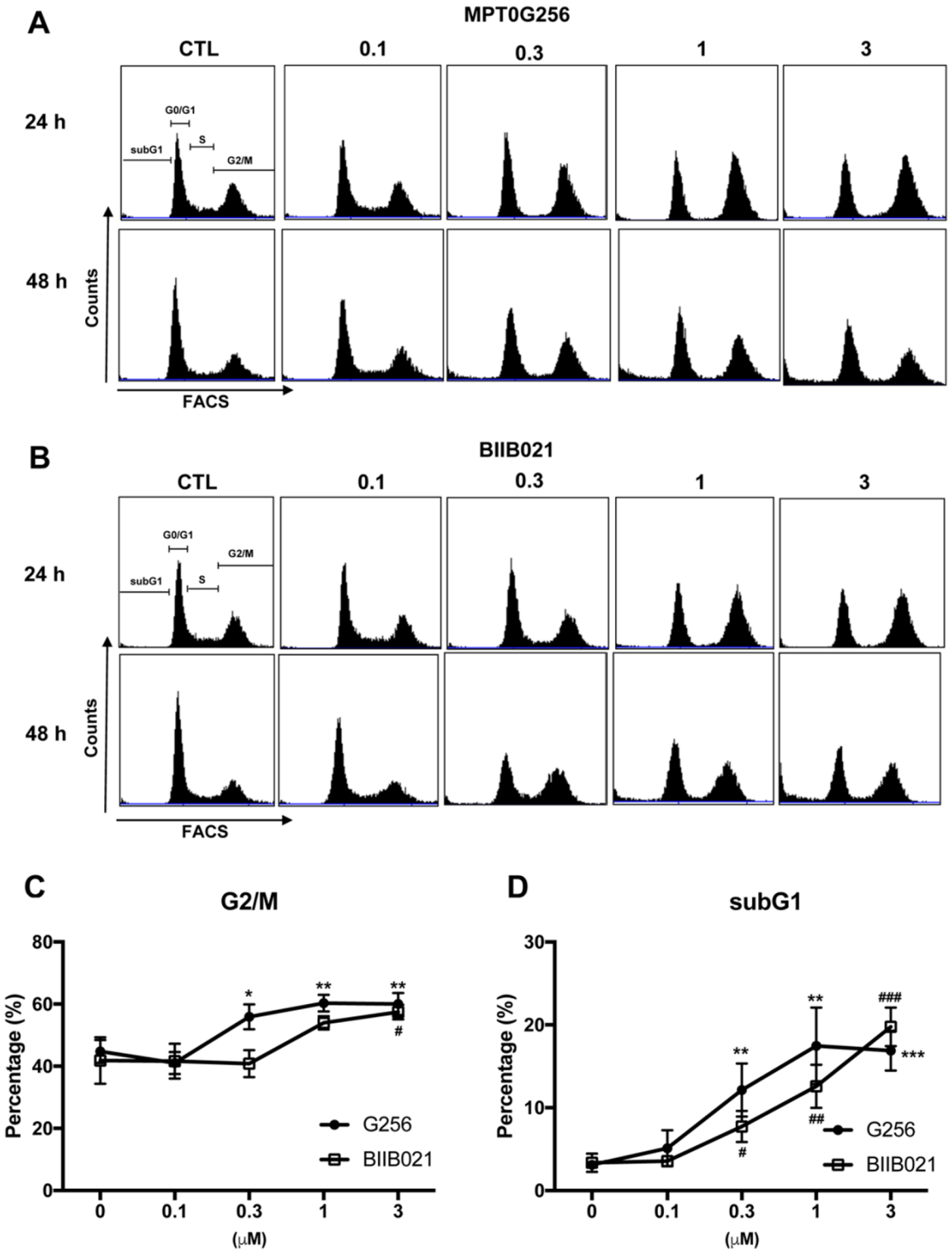

Fig. 4. PC3 cells were treated with DMSO or test compounds, **11** (A) and BIIB021 (B) as the indicated concentrations for 24 h and 48 h. Cells were harvested and analyzed by flow cytometry. The percentage of cell population in G2M (C) and subG1 phase (D). Statistical analysis was performed with the Student *t* test. $^{*}P < 0.05$, $^{**}P < 0.01$, $^{***}P < 0.001$, $^{\#}P < 0.05$, $^{\#\#}P < 0.01$, $^{\#\#\#}P < 0.001$, compared with the control groups. (**MPT0G256** represents **11**).

antiproliferative effects against PC-3 cancer cells. In addition to its induction of HSP90 expression, **11** also downregulates the protein expression levels of client proteins, such as EGFR, Src, FAK, and RB. The significant inhibition of the HSP90 chaperone by **11** was rationalized by its molecular docking into active site of HSP90. The outcome of the present study is consistent with recent reports revealing the promising potential of HSP90 inhibitors against prostate cancer. These are exciting outcomes in light of the fact that prostate cancer is a leading cause of cancer-related mortality and the revelations could be useful for designing chemotherapeutic agents for prostate cancer. Further lead

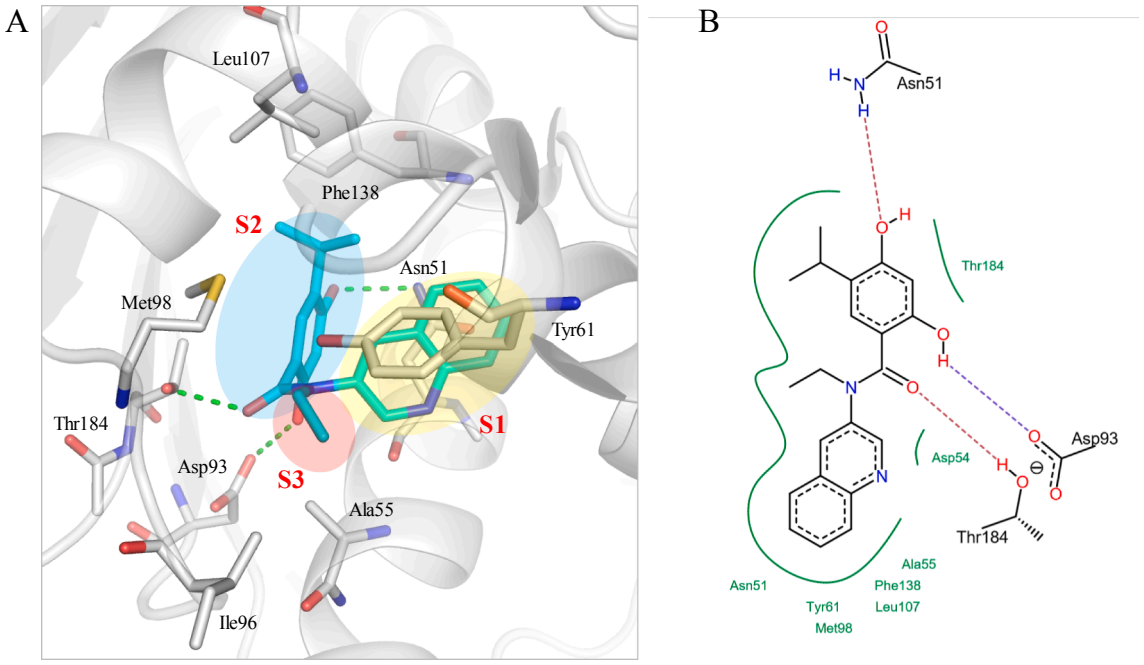

Fig. 5. Molecular docking analysis of **11** in HSP90. (A) **11** (blue) is anchored within the HSP90 (gray) binding site. The three distinct sections of MPTG0G256 are colored as yellow, blue and red, which are located at sites S1, S2 and S3, respectively. Interacting residues are represented as sticks and labeled as shown. Hydrogen bonds are denoted by dotted green lines. (B) A 2D representation of **11** docked in HSP90. Hydrogen bonds are denoted by dashed lines. Green lines represent areas of hydrophobic interactions. Interacting residues are labeled as shown.

modifications on **11** including synthesis of compounds with diverse substitution on the quinoline rings along with positioning of other planar bicyclic heteroaryl rings in the hybrid structure design is under progress.

4. Experimental

4.1. Chemistry

Nuclear magnetic resonance spectra were obtained with Bruker DRX-500 spectrometer operating at 300 MHz, with chemical shift recorded in parts per million (ppm, d) downfield from TMS as an internal standard. High-resolution mass spectra (HRMS) were measured with a JEOL (JMS-700) electron impact (EI) mass spectrometer. Flash column chromatography was accomplished with silica gel (Merck Kieselgel 60, No. 9385, 230e400 mesh ASTM). All reactions were carried out under an atmosphere of dry N_2.

4.1.1. 2,4-Bis(benzyloxy)-5-isopropyl-N-(quinolin-3-yl)benzamide (28)

2,4-Bis(benzyloxy)-5-isopropylbenzoic acid (1.28 g, 3.4 mmol), *N*-methylmorpholine (0.9 mL), 1-ethyl-3-(3-dimethylaminopropyl)carbodiimide) (0.97 g, 5.1 mmol) and hydroxybenzotriazole (0.55 g, 4.1 mmol) were added to a solution of 3-aminoquinoline (**23**) (0.5 g, 3.4 mmol) in DMF (5 mL). The reaction mixture was stirred at rt for

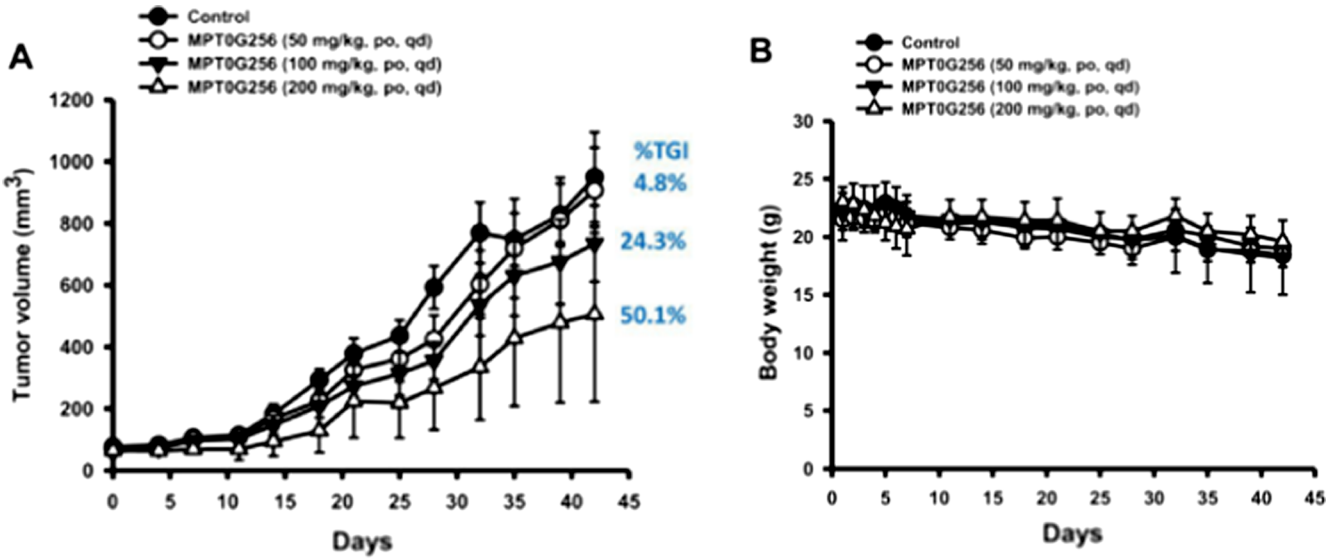

Fig. 6. *In vivo* antitumor activity of 11 in PC3 xenograft model. (A) PC3-tumor-bearing nude mice were treated with vehicle or **11** (50, 100 and 200 mg/kg/d, by oral gavage qd). Tumor was excised when the tumor size reached 1200 mm^3. (B) The body weight of the mice measured daily during the first week and then twice a week of administration. (MPT0G256 represents **11**).

12 h and then diluted with water. Extraction was with EtOAc (3 × 50 mL), and the organic layer was dried over anhydrous $MgSO_4$, filtered, and concentrated. The residue was purified by silica gel chromatography (EtOAc:*n*-hexane = 1:3) to afford compound **6** (1.03 g, 61% yield). ^{1}H NMR (300 MHz, $CDCl_3$) δ 1.29 (d, J = 6.9 Hz, 6H), 3.37 (qui, J = 6.9 Hz, 1H), 5.19 (s, 2H), 5.20 (s, 2H), 7.35–7.64 (m, 13H), 7.74–7.78 (m, 1H), 8.00–8.15 (m, 2H), 8.22 (s, 1H), 8.83 (d, J = 2.4 Hz, 1H), 10.22 (s, 1H).

4.1.2. 2,4-Bis(benzyloxy)-5-isopropyl-N-(2-methylquinolin-4-yl) benzamide (29)

The title compound (**29**) was synthesized in 49% yield in a manner similar to that described for compound **28** using 2-methylquinolin-4-amine (**24**); ^{1}H NMR (300 MHz, MeOD) δ 1.27 (d, J = 6.9 Hz, 6H), 2.68 (s, 3H), 3.34–3.39 (m, 1H), 5.27 (s, 2H), 5.42 (s, 2H), 7.00–7.10 (m, 2H), 7.26–7.62 (m, 12H), 7.86 (d, J = 8.4 Hz, 1H), 8.11 (s, 1H), 8.39 (s, 1H).

4.1.3. 2,4-Bis(benzyloxy)-5-isopropyl-N-(quinolin-5-yl)benzamide (30)

The title compound **30** was synthesized in 54% yield in a manner similar to that described for compound **28** using quinolin-5-amine (**25**); ^{1}H NMR (300 MHz, $CDCl_3$) δ 1.29 (d, J = 6.6 Hz, 6H), 3.38 (qui, J = 6.9 Hz, 1H), 5.20 (s, 2H), 5.22 (s, 2H), 6.72 (s, 1H), 7.00–7.07 (m, 1H), 7.34–7.50 (m, 11*H*), 7.69–7.90 (m, 2H), 8.09 (d, J = 8.4 Hz, 1H), 8.25 (s, 1H), 8.34 (d, J = 7.8 Hz, 1H), 8.8 (d, J = 4.2 Hz, 1H).

4.1.4. 2,4-Bis(benzyloxy)-5-isopropyl-N-(quinolin-6-yl)benzamide (31)

The title compound **31** was synthesized in 53% yield in a manner similar to that described for compound **28** using quinolin-6-amine (**26**); ^{1}H NMR (300 MHz, $CDCl_3$) δ 1.31 (d, J = 6.9 Hz, 6H), 3.38 (qui, J = 6.9 Hz, 1H), 5.16 (s, 4H), 6.63 (s, 1H), 6.96 (dd, J = 6.6, 9 Hz, 1H), 7.24–7.60 (m, 11*H*), 7.86 (d, J = 9 Hz, 1H), 8.01 (d, J = 8.1 Hz, 1H), 8.25–8.30 (m, 2H), 8.75 (dd, J = 2.4, 3.9 Hz, 1H), 10.14 (s, 1H).

4.1.5. 2,4-Bis(benzyloxy)-5-isopropyl-N-(quinolin-8-yl)benzamide (32)

The title compound (**32**) was synthesized in 64% yield in a manner similar to that described for compound **28** using quinolin-8-amine (**27**); ^{1}H NMR (300 MHz, $CDCl_3$) δ 1.20 (d, J = 6.6 Hz, 6H), 3.25 (qui, J = 6.9 Hz, 1H), 4.90 (s, 2H), 5.30 (s, 2H), 6.44 (s, 1H), 7.13–8.19 (m, 13H), 8.33 (m, 1H), 8.34 (s, 1H), 8.99 (d, J = 0.9 Hz, 1H), 9.02 (d, J = 0.9 Hz, 1H), 12.25 (s,1H).

4.1.6. 2,4-Dihydroxy-5-isopropyl-N-(quinolin-3-yl)benzamide (9)

Catalytic Pd/C was added to the solution of compound **28** (0.5 g, 1 mmol) in EtOH (10 mL), and the reaction mixture was stirred at rt under H_2. After continuous stirring for 6 h, the mixture was filtered through celite, dried over anhydrous $MgSO_4$, and then concentrated. The residue was purified by silica gel chromatography (EtOAc:*n*-hexane = 1:1) to afford compound **9** (0.1 g, 31% yield). mp: 232–234 °C. ^{1}H NMR (300 MHz, DMSO-d_6) δ 1.20 (d, J = 6.9 Hz, 6H), 3.13 (qui, J = 6.9 Hz, 1H), 6.43 (s, 1H), 7.55–7.72 (m, 2H), 7.82 (s, 1H), 7.93–8.01 (m, 2H), 8.70 (d, J = 2.4 Hz, 1H), 9.06 (d, J = 2.7 Hz, 1H), 10.22 (s, 1H), 10.58 (s, 1H). HRMS (ESI) for $C_{19}H_{19}N_2O_3$ $[M+H]^+$: calcd, 323.1396; found, 323.1395. LRMS (ESI) $[M+H]^+$: 323.1.

4.1.7. 2,4-Dihydroxy-5-isopropyl-N-(2-methylquinolin-4-yl)benzamide (13)

Catalytic Pd/C, and formic acid (3.2 mL) were added to a solution of compound **29** (0.73 g, 1.41 mmol) in MeOH (15 mL). The resulting mixture was refluxed for 12 h. After cooling at rt, the reaction mixture was filtered through celite and the organic layer was dried over anhydrous $MgSO_4$. The organic layer was then concentrated and the residue was purified by silica gel chromatography (EtOAc:*n*-hexane = 2:1) to afford compound **13** (0.15 g, 31% yield). mp: 216–218 °C. ^{1}H NMR (300 MHz, MeOD) δ 1.23–1.28 (m, 6H), 2.70 (s, 3H), 3.21 (qui, J = 6.9 Hz, 1H), 6.45 (d, J = 1.5 Hz, 1H), 7.54–7.62 (m, 1H), 7.71–7.79 (m, 1H), 7.94 (d, J = 9 Hz, 2H), 8.06 (d, J = 8.4 Hz, 1H), 8.42–8.47 (m, 1H). HRMS (ESI) for $C_{20}H_{21}N_2O_3$ $[M+H]^+$: calcd, 337.1552; found, 337.1555. LRMS (ESI) $[M+H]^+$: 337.1.

4.1.8. 2,4-Dihydroxy-5-isopropyl-N-(quinolin-5-yl)benzamide (15)

Catalytic Pd/C and formic acid (0.9 mL) were added to a solution of compound **30** (0.2 g, 0.40 mmol) in MeOH (15 mL). The reaction mixture was refluxed for 7 h and then cooled at rt. The mixture was filtered through celite, dried over anhydrous $MgSO_4$ and then concentrated. The residue was purified by silica gel chromatography (EtOAc:*n*-hexane = 1:1) to afford compound **15** (0.06 g, 45% yield). mp: 222–224 °C. ^{1}H NMR (300 MHz, MeOD) δ 1.26 (d, J = 7.2 Hz, 6H), 3.18–3.24 (m, 1H), 6.40 (s, 1H), 7.56–7.63 (m, 1H), 7.78–7.99 (m, 4H), 8.48 (d, J = 9 Hz, 1H), 8.88 (d, J = 3.9 Hz, 1H). HRMS (ESI) for $C_{19}H_{19}N_2O_3$ $[M+H]^+$: calcd, 323.1396; found, 323.1395. LRMS (ESI) $[M+H]^+$: 323.1.

4.1.9. 2,4-Dihydroxy-5-isopropyl-N-(quinolin-6-yl)benzamide (17)

The title compound **17** was synthesized in 63% yield using compound **31** in a manner similar to that described for compound **9**; mp: 162–164 °C; ^{1}H NMR (300 MHz, DMSO-d_6) δ 1.20 (d, J = 6.9 Hz, 6H), 3.14 (qui, J = 6.9 Hz, 1H), 6.43 (s, 1H), 7.50 (q, J = 4.2 Hz, 1H), 7.82 (s, 1H), 7.92–8.05 (m, 2H), 8.28–8.42 (m, 2H), 8.78–8.84 (m, 1H), 10.18 (s, 1H), 10.46 (s, 1H). HRMS (ESI) for $C_{19}H_{19}N_2O_3$ $[M+H]^+$: calcd, 323.1396; found, 323.1396. LRMS (ESI) $[M+H]^+$: 323.1.

4.1.10. 2,4-Dihydroxy-5-isopropyl-N-(quinolin-8-yl)benzamide (20)

The title compound **20** was synthesized in 52% yield using compound **32** in a manner similar to that described for compound **9**; mp: 172–174 °C; ^{1}H NMR (300 MHz, MeOD) δ 1.27 (d, J = 6.9 Hz, 6H), 3.23 (qui, J = 6.9 Hz, 1H), 6.41 (s, 1H), 7.49–7.60 (m, 3H), 7.81 (s, 1H), 8.26 (dd, J = 1.8, 8.4 Hz, 1H), 8.80 (dd, J = 2.1, 6.9 Hz, 1H), 8.85 (dd, J = 1.5, 4.2 Hz, 1H). HRMS (ESI) for $C_{19}H_{19}N_2O_3$ $[M+H]^+$: calcd, 323.1396; found, 323.1389. LRMS (ESI) $[M+H]^+$: 323.1.

4.1.11. 2,4-Bis(benzyloxy)-5-isopropyl-N-methyl-N-(quinolin-3-yl) benzamide (33)

Cesium carbonate (0.65 g, 1.98 mmol) was added to a solution of compound **28** (1 g, 1.98 mmol) in MeCN (5 mL). The mixture was stirred for 30 min before adding MeI (0.246 mL, 3.96 mmol). The reaction mixture was stirred for 12 h and then diluted with water. The mixture was extracted with EtOAc and the organic layer was dried over anhydrous $MgSO_4$, filtered, and concentrated. The mixture was purified by silica gel chromatography (EtOAc:*n*-hexane = 1:4) to afford compound **33** (0.08 g, 8% yield). ^{1}H NMR (300 MHz, $CDCl_3$) δ 1.12 (d, J = 6.9 Hz, 6H), 3.14–3.29 (m, 1H), 3.51 (s, 3H), 4.72 (s, 2H), 4.84 (s, 2H), 7.24–7.40 (m, 11*H*), 7.48–7.56 (m, 3H), 7.60–7.70 (m, 2H), 8.00 (d, J = 9.0 Hz, 1H), 8.53 (s, 1H).

4.1.12. 2,4-Bis(benzyloxy)-N-ethyl-5-isopropyl-N-(quinolin-3-yl) benzamide (34)

Sodium hydride (0.05 g, 2 mmol) was added to a solution of compound **28** (0.5 g, 1 mmol) in DMF (5 mL), and the reaction mixture was stirred for 20 min at 0 °C. EtI (0.25 mL, 3.10 mmol) was then added and stirring was continued for 4 h at rt. The reaction mixture was diluted with water and extracted with EtOAc. The organic layer was dried over anhydrous $MgSO_4$, filtered, and concentrated. The residue obtained was used in a subsequent reaction without purification.

4.1.13. 2,4-Bis(benzyloxy)-5-isopropyl-N-propyl-N-(quinolin-3-yl) benzamide (35)

Potassium *t*-butoxide (0.15 g, 1.35 mmol) was added to a solution of compound **28** (0.45 g, 0.9 mmol) in THF (5 mL). The mixture was stirred for 10 min before adding *n*-PrI (0.437 mL, 4.48 mmol). The reaction mixture was then stirred at rt for 5 h. Water was added to the

reaction mixture which was then extracted with EtOAc. The organic layer was dried over anhydrous $MgSO_4$, filtered, and concentrated. The mixture was purified by silica gel chromatography (EtOAc:*n*-hexane = 1:3) to afford compound **35** (0.44 g, 90% yield). ^{1}H NMR (300 MHz, $CDCl_3$) δ 0.86–0.96 (m, 3H), 1.13 (d, J = 6.6 Hz, 6H), 1.58–1.68 (m, 2H), 3.20 (t, J = 6.6 Hz, 1H), 3.92 (s, 2H), 4.76 (s, 2H), 4.83 (s, 2H), 6.15 (s, 1H), 7.25–7.40 (m, 11*H*), 7.45–7.57 (m, 2H), 7.60–7.69 (m, 2H), 8.02 (d, J = 8.4 Hz, 1H), 8.54 (s, 1H).

*4.1.14. 2, 4-Bis(benzyloxy)-N-ethyl-5-isopropyl-N-(quinolin-6-yl)benzamide (**36**)*

The title compound **36** was synthesized in 85% yield in a manner similar to that described for compound **35** using compound **31**; ^{1}H NMR (300 MHz, $CDCl_3$) δ 0.99 (d, J = 6.9 Hz, 6H), 1.13 (m, 5H), 3.06–3.15 (m, 1H), 3.91 (d, J = 6.0 Hz, 2H), 4.73 (d, J = 14.1 Hz, 4H), 7.06–7.28 (m, 13H), 7.75 (t, J = 6.9 Hz, 2H), 8.73 (dd, J = 1.5, 3.9 Hz, 1H).

*4.1.15. 2,4-Bis(benzyloxy)-N-ethyl-5-isopropyl-N-(quinolin-8-yl) benzamide (**37**)*

The title compound **37** was synthesized in 43% yield in a manner similar to that described for compound **35** using compound **32**; ^{1}H NMR (300 MHz, $CDCl_3$) δ 0.4 (d, J = 6.9 Hz, 3H), 0.87 (d, J = 6.6 Hz, 3H), 1.20 (t, J = 7.2 Hz, 3H), 3.62–3.73 (m, 1H), 4.59–4.66 (m, 1H), 4.77 (s, 2H), 4.90–5.05 (m, 2H), 6.18 (s, 1H), 6.84 (s, 1H), 7.20–7.47 (m, 14H), 7.59 (d, J = 8.1 Hz, 1H), 8.03 (d, J = 7.2 Hz, 1H), 8.98 (d, J = 2.7 Hz, 1H).

*4.1.16. 2,4-Dihydroxy-5-isopropyl-N-methyl-N-(quinolin-3-yl)benzamide (**10**)*

The title compound **10** was synthesized in 79% yield in a manner similar to that described for compound **9** using compound **33**; mp: 236–238 °C; ^{1}H NMR (300 MHz, $(CD_3)_2CO$) δ 1.27 (d, J = 7.2 Hz, 6H), 3.26 (qui, J = 7.2 Hz, 1H), 3.84 (s, 3H), 6.53 (s, 1H), 7.29–7.37 (m, 1H), 7.55–7.59 (m, 2H), 7.70–7.77 (m, 2H), 8.82 (s, 1H), 9.20 (s, 1H), 10.20 (s, 1H), 11.35 (s, 1H). HRMS (ESI) for $C_{20}H_{21}N_2O_3$ $[M+H]^+$: calcd, 337.1552; found, 337.1554. LRMS (ESI) $[M+H]^+$: 337.1.

*4.1.17. N-Ethyl-2,4-dihydroxy-5-isopropyl-N-(quinolin-3-yl)benzamide (**11**)*

Catalytic Pd/C and formic acid (0.9 mL) were added to a solution of compound **34** (0.21 g, 0.39 mmol) in MeOH (15 mL). The resulting mixture was refluxed for 12 h and then cooled to rt. The mixture was filtered through celite, dried over anhydrous $MgSO_4$ and then concentrated. Purification was done by silica gel chromatography (EtOAc:*n*-hexane = 1:4) to afford compound **11** (0.10 g, 73% yield); mp: 207–209 °C; ^{1}H NMR (300 MHz, MeOD) δ 0.70 (d, J = 6.9 Hz, 6H), 1.26 (t, J = 7.2 Hz, 3H), 2.80–2.94 (m, 1H), 4.04–4.14 (m, 2H), 6.11 (s, 1H), 6.67(s, 1H), 7.57–7.65 (m, 1H), 7.70–7.79 (m, 1H), 7.88 (d, J = 8.4 Hz, 1H), 7.96 (d, J = 8.7 Hz, 1H), 8.21 (d, J = 2.4 Hz, 1H), 8.55 (d, J = 2.4 Hz, 1H). HRMS (ESI) for $C_{21}H_{23}N_2O_3$ $[M+H]^+$: calcd, 351.1709; found, 351.1706. LRMS (ESI) $[M+H]^+$: 351.1.

*4.1.18. 2,4-Dihydroxy-5-isopropyl-N-propyl-N-(quinolin-3-yl)benzamide (**12**)*

The title compound **12** was synthesized in 13% yield in a manner similar to that described for compound **13** using compound **35**; mp: 197–199 °C; ^{1}H NMR (300 MHz, $CDCl_3$) δ 0.42 (d, J = 6.9 Hz, 6H), 0.96 (t, J = 7.2 Hz, 3H), 1.65–1.79 (m, 2H), 2.75 (qui, J = 6.9 Hz, 1H), 3.93–4.01 (m, 2H), 6.29 (s, 1H), 6.37 (s, 1H), 7.53–7.63 (m, 1H), 7.67–7.81 (m, 2H), 7.96 (d, J = 2.4 Hz, 1H), 8.08 (d, J = 8.4 Hz, 1H), 8.58 (d, J = 2.7 Hz, 1H), 10.93 (s, 1H). HRMS (ESI) for $C_{22}H_{23}N_2O_3$ $[M-H]^+$: calcd, 363.1709; found, 363.1727. LRMS (ESI) $[M]^+$: 364.9.

*4.1.19. N-Ethyl-2,4-dihydroxy-5-isopropyl-N-(quinolin-6-yl)benzamide (**19**)*

Catalytic Pd/C was added to a solution of compound **36** (0.36 g, 0.68 mmol) in MeOH (3 mL) and THF (10 mL), The reaction mixture was stirred at rt for 5 h under H_2 and then filtered through celite. The organic layer was dried over anhydrous $MgSO_4$, concentrated and the residue obtained was purified by silica gel chromatography (EtOAc:*n*-hexane = 1:2) to afford compound **19** (0.09 g, 38% yield); mp: 220–221 °C; ^{1}H NMR (300 MHz, DMSO-d_6) δ 0.57 (d, J = 6.6 Hz, 6H), 1.14 (t, J = 6.9 Hz, 3H), 2.71–2.77 (m, 1H), 3.93 (q, J = 6.9 Hz, 2H), 6.12 (s, 1H), 6.53 (s, 1H), 7.49 (q, J = 4.2 Hz, 1H), 7.58 (dd, J = 2.4, 9 Hz, 1H), 7.76 (d, J = 2.4 Hz, 1H), 7.94 (d, J = 9 Hz, 1H), 8.23–8.28 (m, 1H), 8.83–8.87 (m, 1H). HRMS (ESI) for $C_{21}H_{23}N_2O_3$ $[M+H]^+$: calcd, 351.1709; found, 351.1711. LRMS (ESI) $[M+H]^+$: 351.1.

*4.1.20. N-Ethyl-2,4-dihydroxy-5-isopropyl-N-(quinolin-8-yl)benzamide (**22**)*

The title compound **22** was synthesized in 66% yield in a manner similar to that described for compound **13** using compound **37**; mp: 82–84 °C; ^{1}H NMR (300 MHz, $CDCl_3$) δ 0.39 (bs, 6H), 1.21 (qui, J = 7.2 Hz, 3H), 2.66 (m, 1H), 4.10 (q, J = 7.2 Hz, 2H), 6.20 (s, 1H), 6.40 (s, 1H), 6.46 (s, 1H), 7.25–7.50 (m, 3H), 7.75 (dd, J = 1.8, 7.8 Hz, 1H), 8.19 (dd, J = 1.8, 8.4 Hz, 1H), 8.96 (dd, J = 1.8, 4.2 Hz, 1H), 11.23 (s, 1H). HRMS (ESI) for $C_{21}H_{23}N_2O_3$ $[M+H]^+$: calcd, 351.1709; found, 351.1711. LRMS (ESI) $[M+H]^+$: 351.1.

*4.1.21. 4-((tert-Butyldimethylsilyl)oxy)-2-hydroxy-5-isopropyl-N-(2-methylquinolin-4-yl)benzamide (**38**)*

tert-Butyldimethylsilyl chloride (0.13 g, 0.89 mmol) and N,*N*-diisopropylethylamine (0.12 g, 0.89 mmol) were added to a solution of compound **13** (0.15 g, 0.44 mmol) in dry CH_2Cl_2 (5 mL). The reaction mixture was stirred at rt for 6 h and then water was added. The organic layer was separated, dried over anhydrous $MgSO_4$, and concentrated. The residue was purified by silica gel chromatography (EtOAc:*n*-hexane = 1:1) to afford compound **38** (0.11 g, 54% yield). ^{1}H NMR (300 MHz, $CDCl_3$) δ 0.07 (s, 6H), 0.92 (s, 9H), 1.24 (d, J = 6.9 Hz, 6H), 2.80 (s, 3H), 3.17–3.27 (m, 1H), 6.49 (s, 1H), 7.40 (t, J = 7.2 Hz, 1H), 7.62 (t, J = 8.1 Hz, 1H), 7.84 (s, 1H), 8.00–8.10 (m, 2H), 8.53 (s, 1H), 10.89 (m, 1H).

*4.1.22. 4-((tert-Butyldimethylsilyl)oxy)-2-hydroxy-5-isopropyl-N-(quinolin-5-yl)benzamide (**39**)*

The title compound **39** was synthesized in 58% yield in a manner similar to that described for compound **38** using compound **15** ; ^{1}H NMR (300 MHz, $CDCl_3$) δ 0.28 (s, 6H), 1.02 (s, 9H), 1.23 (d, J = 6.9 Hz, 7H), 3.26 (qui, J = 6.9 Hz, 1H), 6.46 (s, 1H), 7.40 (q, J = 4.2 Hz, 1H), 7.60 (s, 1H), 7.66–7.77 (m, 2H), 8.01–8.06 (m, 1H), 8.29 (d, J = 7.8 Hz, 1H), 8.78 (s, 1H), 8.84–8.88 (m, 1H).

*4.1.23. 4-((tert-Butyldimethylsilyl)oxy)-2-hydroxy-5-isopropyl-N-(quinolin-6-yl)benzamide (**40**)*

The title compound **40** was synthesized in 45% yield in a manner similar to that described for compound **38** using compound **17**. ^{1}H NMR (300 MHz, $CDCl_3$) δ 0.39 (s, 6H), 1.03 (s, 9H), 1.25 (d, J = 6.9 Hz, 7H), 3.26 (qui, J = 6.9 Hz, 1H), 6.46 (s, 1H), 7.35 (s, 1H), 7.43 (q, J = 4.2 Hz, 1H), 7.75 (dd, J = 2.4, 9 Hz, 1H), 8.10–8.21 (m, 2H), 8.35 (d, J = 2.1 Hz, 1H), 8.86–8.92 (m, 1H), 12.06 (s, 1H).

*4.1.24. 4-((tert-Butyldimethylsilyl)oxy)-2-hydroxy-5-isopropyl-N-(quinolin-8-yl)benzamide (**41**)*

The title compound **41** was synthesized in 25% yield in a manner similar to that described for compound **38** using compound **20**; ^{1}H NMR (300 MHz, $CDCl_3$) δ 0.31 (d, J = 7.2 Hz, 6H), 1.05 (s, 9H), 1.32 (d, J = 6.9 Hz, 6H), 3.25–3.36 (m, 1H), 7.54 (m, 4H), 8.18 (dd, J = 1.5, 8.1 Hz, 1H), 8.78 (dd, J = 1.8, 6.9 Hz, 1H), 8.87 (dd, J = 1.5, 4.2 Hz, 1H), 10.85 (s, 1H), 12.33 (s, 1H).

*4.1.25. 4-((tert-Butyldimethylsilyl)oxy)-N-ethyl-2-hydroxy-5-isopropyl-N-(2-methylquinolin-4-yl)benzamide (**42**)*

Potassium *t*-butoxide (0.02 g, 0.17 mmol) was added to a solution of

compound **38** (0.05 g, 0.11 mmol) in THF (5 mL). The mixture was stirred for 10 min before adding EtI (0.77 mL). Stirring was continued at rt for another 6 h. The reaction mixture was diluted with water, extracted with EtOAc, and the organic layer was dried over anhydrous $MgSO_4$, filtered, and concentrated. The mixture was purified by silica gel chromatography (EtOAc:*n*-hexane = 1:1) to afford compound **42** (0.015 g, 36% yield). ^{1}H NMR (300 MHz, $CDCl_3$) δ 0.31 (s, 6H), 1.05 (s, 9H), 1.24 (d, J = 6.9 Hz, 6H), 1.67 (t, J = 6.9 Hz, 3H), 2.91 (s, 3H), 3.24 (qui, J = 6.9 Hz, 1H), 4.34 (qui, J = 6.9 Hz, 2H), 6.51 (s, 1H), 7.61 (t, J = 8.1 Hz, 1H), 7.80 (t, J = 6.9 Hz, 1H), 7.99 (d, J = 8.4 Hz, 1H), 8.19 (s, 1H), 8.45 (br, 1H), 8.68 (s, 1H).

*4.1.26. 4-((tert-Butyldimethylsilyl)oxy)-2-hydroxy-5-isopropyl-N-methyl-N-(quinolin-5-yl)benzamide (**43**)*

The title compound **43** was synthesized in 64% yield in a manner similar to that described for compound **42** using compound **39**; ^{1}H NMR (300 MHz, $CDCl_3$) δ 0.31 (s, 6H), 1.06 (s, 9H), 1.24 (d, J = 6.9 Hz, 6H), 3.25(qui, J = 6.9 Hz, 1H), 4.08 (s, 3H), 6.51 (s, 1H), 7.45 (q, J = 4.2 Hz, 1H), 7.75 (t, J = 7.8 Hz, 1H), 7.95 (d, J = 8.4 Hz, 1H), 8.21–8.34 (m, 3H), 8.94 (dd, J = 1.5, 3.9 Hz, 1H), 10.18 (s, 1H).

*4.1.27. 4-((tert-Butyldimethylsilyl)oxy)-2-hydroxy-5-isopropyl-N-methyl-N-(quinolin-6-yl)benzamide (**44**)*

The title compound **44** was synthesized in 88% yield in a manner similar to that described for compound **42** using compound **40**; ^{1}H NMR (300 MHz, $CDCl_3$) δ 0.30 (s, 6H), 1.04 (d, J = 3 Hz, 9H), 1.23 (d, J = 6.9 Hz, 6H), 3.24 (qui, J = 6.9 Hz, 1H), 4.03 (s, 3H), 6.45 (s, 1H), 7.35–7.40 (m, 1H), 7.59 (dd, J = 2.4, 9 Hz, 1H), 8.05 (d, J = 9 Hz, 1H), 8.12–8.17 (m, 1H), 8.19 (s, 1H), 8.64 (d, J = 2.1 Hz, 1H), 8.78–8.85 (m, 1H), 10.00 (s, 1H).

*4.1.28. 4-((tert-Butyldimethylsilyl)oxy)-2-hydroxy-5-isopropyl-N-methyl-N-(quinolin-8-yl)benzamide (**45**)*

The title compound **45** was synthesized in 68% yield in a manner similar to that described for compound **42** using compound **41**. ^{1}H NMR (300 MHz, $CDCl_3$) δ 0.31 (s, 6H), 1.05 (s, 9H), 1.24 (d, J = 6.9 Hz, 6H), 3.25 (qui, J = 6.9 Hz, 1H), 4.14 (s, 3H), 6.49 (s, 1H), 7.45–7.62 (m, 3H), 8.15–8.23 (m, 2H), 8.87 (dd, J = 1.5, 4.2 Hz, 1H), 9.03 (dd, J = 1.5, 7.8 Hz, 1H), 12.25 (s, 1H).

*4.1.29. N-Ethyl-2,4-dihydroxy-5-isopropyl-N-(2-methylquinolin-4-yl) benzamide (**14**)*

Tetra-*n*-butylammonium fluoride (0.07 mL) was added to a solution of compound **42** (0.03 g, 0.06 mmol) in dry DCM (3 mL). The reaction mixture was stirred at rt for 6 h and then diluted with water. Extraction was carried out with DCM and the organic layer was dried over anhydrous $MgSO_4$, filtered, and concentrated. The residue was purified by silica gel chromatography (EtOAc:*n*-hexane = 1:1) to afford compound **14** (0.02 g, 55% yield). ^{1}H NMR (300 MHz, MeOD) δ 1.25 (d, J = 7.2 Hz, 6H), 1.62 (t, J = 7.2 Hz, 3H), 2.71 (s, 3H), 3.19–3.28 (m, 1H), 4.38 (q, J = 7.2 Hz, 2H), 6.62 (s, 1H), 7.59–7.67 (m, 1H), 7.75–7.83 (m, 1H), 7.94–8.09 (m, 3H), 8.45 (s, 1H). HRMS (ESI) for $C_{22}H_{23}N_2O_3$ [M-H] $^+$: calcd, 363.1709; found, 363.1717. LRMS (ESI) [M] $^+$: 364.9.

*4.1.30. 2,4-Dihydroxy-5-isopropyl-N-methyl-N-(quinolin-5-yl)benzamide (**16**)*

The title compound **16** was synthesized in 71% yield in a manner similar to that described for compound **14** using compound **43**; ^{1}H NMR (300 MHz, MeOD) δ 1.22–1.30 (m, 6H), 3.20–3.28 (m, 1H), 4.09 (s, 3H), 6.63 (s, 1H), 7.63 (q, J = 4.5 Hz, 1H), 7.84 (m, 1H), 7.95 (m, 2H), 8.06 (d, J = 7.5 Hz, 1H), 8.48 (dd, J = 1.2, 8.4 Hz, 1H), 8.87–8.91 (m, 1H). HRMS (ESI) for $C_{20}H_{19}N_2O_3$ [M]$^-$: calcd, 335.1396; found, 335.1410. LRMS (ESI) [M] $^+$: 336.9.

*4.1.31. 2,4-Dihydroxy-5-isopropyl-N-methyl-N-(quinolin-6-yl)benzamide (**18**)*

The title compound **18** was synthesized in 40% yield in a manner similar to that described for compound **14** using compound **44**; mp: 277–279 °C. ^{1}H NMR (300 MHz, DMSO-d_6) δ 1.17 (d, J = 6.9 Hz, 6H), 3.10–3.22 (m, 1H), 3.93 (s, 3H), 6.60 (s, 1H), 7.46–7.53 (m, 1H), 7.69 (s, 1H), 7.93–7.99 (m, 2H), 8.28 (dd, J = 1.5, 8.4 Hz, 1H), 8.51 (d, J = 1.5 Hz, 1H), 8.76–8.82 (m, 1H), 10.13 (s, 1H). HRMS (ESI) for $C_{20}H_{21}N_2O_3$ [M + H] $^+$: calcd, 337.1552; found, 337.1553. LRMS (ESI) [M + H] $^+$: 337.1.

*4.1.32. 2,4-Dihydroxy-5-isopropyl-N-methyl-N-(quinolin-8-yl)benzamide (**21**)*

The title compound **21** was synthesized in 54% yield in a manner similar to that described for compound **14** using compound **45**; ^{1}H NMR (300 MHz, $(CD_3)_2CO$) δ 1.27 (d, J = 6.9 Hz, 6H), 3.03 (qui, J = 6.9 Hz, 1H), 4.17 (s, 3H), 6.73 (s, 1H), 7.56–7.62 (m, 3H), 8.15 (s, 1H), 8.34 (dd, J = 1.5, 8.1 Hz, 1H), 8.96–9.07 (m, 2H), 12.33 (s, 1H). HRMS (ESI) for $C_{20}H_{21}N_2O_3$ [M + H] $^+$: calcd, 337.1552; found, 337.1558. LRMS (ESI) [M + H] $^+$: 337.1.

4.2. Cell culture

Human cancer cells were purchased from the American Type Culture Collection (Manassas, VA, USA). These cell lines were cultured in RPMI 1640 medium or DMEM supplemented with 10% FBS (v/v) and penicillin (100 U/mL)/streptomycin (100 μg/mL)/amphotericin B (0.25 μg/mL). Cultures were maintained at 37 °C in a humidified atmosphere of 5% CO2/95% air.

4.2.1. SRB assay

Cells were seeded in 96-well plates in their cultured medium. After 24 h, cells were fixed with 10% trichloroacetic acid to represent cell population at the time of drug addition (*T*0). After incubation of DMSO or test compounds for 48 h, cells were fixed with 10% trichloroacetic acid and sulforhodamine B at 0.4% (w/v) in 1% AcOH was added to stain cells. Unbound sulforhodamine B was washed out with 1% AcOH and sulforhodamine B–bound cells were solubilized with 10 mmol/L Trizma base. The absorbance was read at a wavelength of 515 nm. Using the following absorbance measurements, such as time zero (*T*0), control growth (*C*), and cell growth in the presence of the drug (*Tx*), the percentage growth was calculated at each of the compound concentrations levels. Percentage growth inhibition was calculated as 100 - $[(Tx - T0)/(C - T0)] \times 100$. Growth inhibition of 50% (GI_{50}) is determined at the drug concentration that results in 50% reduction of total protein increase in control cells during the compound incubation.

4.3. In vitro Hsp90α assay

To assess the effects on HSP90 activity *in vitro*, Hsp90α Assay Kits (BPS Bioscience, San Diego, CA, USA) were used. Following the instruction manual, master mixture (Hsp90 assay buffer, DTT, BSA and H_2O) and FITC-labeled geldanamycin were added to all 96 wells. Then test compounds were added to each well designated "Test Inhibitor". To the "Blank", "Enzyme Positive Control" and "Enzyme Negative Control" wells, the same solution with inhibitor was added. To the "Enzyme Negative Control" and "Blank" wells, HSP90 assay buffer was added. Finally, the recombinant protein Hsp90α was incubated in every well designated "Enzyme Positive Control" and "Test Inhibitor" for 2–3 h at rt with slow shaking. The fluorescent polarization of the samples was determined by microtiter-plate reader, which can detect excitation ranging from 475 to 495 nm and emission ranging from 518 to 538 nm.

4.4. Western blot assay

For Western blot analysis, cells were treated with the indicated concentrations of drugs for 24 and 48 h and then harvested by scraping

with lysis buffer (1 mM EGTA, 1 mM EDTA, 150 mM NaCl, 1% Triton X-100, 2.5 mM sodium pyrophosphate, 1 mM PMSF, 1 mM Na3VO4, 1 μg/mL leupeptin, 1 μg/mL aprotinin, 5 mM NaF in 20 mM Tris–HCl buffer, pH 7.5). Cell lysates were centrifuged at 13,000*g* for 30 min. Total protein was determined and equal amounts of protein were separated by SDS–PAGE and immunoblotted with specific antibodies. Proteins were visualized with enhanced chemiluminescence (Amersham, Buckinghamshire, UK).

4.5. Cell cycle analysis

PC3 cells were seeded on 6-well plates (2.5×10^5/well) and treated with the indicated drugs and concentrations for 24 and 48 h. Then the cells were harvested and trypsinized, washed with PBS (phosphate-buffered saline) and fixed in cold 70% EtOH for at least 30 min at 4 °C. After removal of EtOH by spinning at 2000 rpm for 30 min in a centrifuge, the pellets were resuspended in DNA extract buffer (0.2 M Na_2HPO_4, 0.1 M citric acid; pH 7.8) for 20 min. Then the cells were washed with PBS and stained with propidium iodide (PI, 100 μg/ml RNaseA, 80 μg/ml propidium iodide, 0.1% Triton X-100 in PBS). Cell cycle distribution was measured by BD Accuri™ and C6 Software (BD Biosciences, Franklin Lakes, NJ, USA).

4.6. Molecular modeling studies

The crystal structure of HSP90 (PDB ID: 5GGZ) was downloaded from the Protein Data Bank [36] The drug design platform, Lead IT [37] was used for docking analysis. The Lead IT software was also used to prepare the target protein. The target protein was prepared by removing the co-crystal ligand and water molecules. Compounds were protonated in aqueous solution. The binding site was defined as a radius of 10 Å using the co-crystallized ligand as a reference. A hybrid (enthalpy and entropy) docking strategy was used. All scoring parameters were used with the default settings.

4.7. Mice xenograft model

Adult (5–6 weeks old) nude male mice were purchased from National Laboratory Animal Center (NLAC) of Taiwan. During experimental period, the mice were housed at the Laboratory Animal Center of Taipei Medical University, on a 12-hour light cycle at 21–23 °C and 60–85% humidity. The cancer cells were harvested and resuspended in PBS at 5×10^7 cells/mL. Each mouse was injected s.c. in the right flank with 1×10^7 cells (0.2 mL cell suspension). The tumor size and body weight were monitored twice weekly until their volumes approached 1,200 mm^3. On D1 of the study the animals were sorted into treatment groups with tumor sizes of 60–150 mm^3. Tumor size, in mm^3, was calculated as: Tumor Volume = $w2 \times l/2$ where w = width and l = length in mm of the tumor. All treatment doses were administered at a volume of 10 mL/kg (0.2 mL/20 g mouse), scaled to the body weight of each animal. Control mice receive vehicle treatment (1% CMC and 0.5% Tween80 in ddH_2O). All experiments were maintained in accordance with the Institutional Animal Care and Use Committee procedures and guidelines.

Acknowledgments

This research was supported by the Ministry of Science and Technology, Taiwan (grant no. MOST 107-2113-M-038-001) and Taipei Medical University, Taiwan (grant no. TMU 107-AE1-B33).

Appendix A. Supplementary material

Supplementary data to this article can be found online at https://doi.org/10.1016/j.bioorg.2019.103119.

References

[1] L. Whitesell, S.L. Lundquist, Hsp90 and the chaperoning of cancer, Nat. Rev. Can. 5 (2005) 761–1572.
[2] (a) C. Jolly, R.I. Morimoto, Role of the heat shock response and molecular chaperones in oncogenesis and cell death, J. Natl. Can. Inst. 92 (2000) 1564–1572; (b) S. Walter, J. Buchner, Molecular chaperones-cellular machines for protein folding, Angew. Chem. Int. Ed. Engl. 41 (2002) 1098–1113.
[3] J.C. Young, V.R. Agashe, K. Siegers, F.U. Hartl, Pathways of chaperone-mediated protein folding in the cytosol, Nat. Rev. Mol. Cell Biol. 5 (2004) 781–791.
[4] (a) N. Wayne, P. Mishra, D.N. Bolon, Hsp90 and client protein maturation, Methods Mol. Biol. 787 (2011) 33–44; (b) D. Hanahan, R.A. Weinberg, The hallmark of cancer, Cell 100 (2000) 57–70.
[5] (a) J.H. Jeong, Y.J. Oh, Y. lho, Y.P. Sun, K.H. Liu, E. Ha, Y.H. Seo, Targeting the entry region of Hsp90's ATP binding pocket with a novel 6,7-dihydrothieno[3,2-c] pyridin-5(4H)-yl amide, Eur. J. Med. Chem. 124 (2016) 1069–1080; (b) U. Banerji, A. O'Donnell, M. Scurr, S. Pacey, S. Stapleton, Y. Asad, L. Simmons, A. Maloney, F. Raynaud, M. Campbell, Phase I pharmacokinetic and pharmacodynamic study of 17-allylamino, 17-demethoxygeldanamycin in patients with advanced malignancies, J. Clin. Oncol. 23 (2005) 4152–4161.
[6] S. Chatterjee, S. Bhattacharya, M.A. Socinski, T.F. Burns, HSP90 inhibitors in lung cancer: promise still unfulfilled, Clin. Adv. Hematol. Oncol. 14 (2016) 346–356.
[7] M. Ferrarini, S. Heltai, M.R. Zocchi, C. Rugarli, Unusual expression and localization of heat-shock proteins in human tumor cells, Intl. J. Cancer 51 (1992) 613–619.
[8] S.Y. Park, Y.J. Oh, Y. Lho, J.H. Jeong, K.H. Liu, J. Song, S.H. Kim, E. Ha, Y.H. Seo, Design, synthesis, and biological evaluation of a series of resorcinol-based N-benzyl benzamide derivatives as potent Hsp90 inhibitors, Eur. J. Med. Chem. 143 (2018) 390–401.
[9] (a) H.K. Armstrong, J.L. Gillis, I.R.D. Johnson, Z.D. Nassar, M. Moldovan, C. Levrier, M.C. Sadowski, M.Y. Chin, E.S.T. Guns, G. Tarulli, D.J. Lynn, D.A. Brooks, L.A. Selth, M.M. Centenera, L.M. Butler, Dysregulated fibronectin trafficking by Hsp90 inhibition restricts prostate cancer cell invasion, Sci. Rep. 8 (2018) 2090; (b) D.B. Solit, H.I. Scher, N. Rosen, Hsp90 as a therapeutic target in prostate cancer, Semin. Oncol. 30 (2003) 709–716; (c) L. Chen, J. Li, E. Farah, S. Sarkar, N. Ahmad, S. Gupta, J. Larner, X. Liu, Cotargeting HSP90 and its client proteins for treatment of prostate cancer, Mol. Cancer Ther. 15 (2016) 2107–2118; (d) M.M. Centenera, A.K. Fitzpatrick, W.D. Tilley, L.M. Butler, Hsp90: still a viable target in prostate cancer, Biochim Biophys Acta. 2013 (1835) 211–218; (e) M.R. Woodford, A. Madala, J. Schulman, T. Nsouli, M. Mollapour, Efficacy of the Hsp90 inhibitors in prostate cancer therapy, J. Urol. Nephrol. 1 (1) (2014) 9; (f) J. Wang, Z. Li, Z. Lin, B. Zhao, Y. Wang, R. Peng, M. Wang, C. Lu, G. Shi, Y. Shen, 17-DMCHAG, a new geldanamycin derivative, inhibits prostate cancer cells through Hsp90 inhibition and survivin downregulation, Cancer Lett. 362 (2015) 83–96; (g) W. Hessenkemper, A. Baniahmad, Targeting heat shock proteins in prostate cancer, Curr. Med. Chem. 20 (2013) 2731–2740.
[10] L. Chen, J. Li, E. Farah, S. Sarkar, N. Ahmad, S. Gupta, J. Larner, X. Liu, Co-targeting HSP90 and its client proteins for treatment of prostate cancer, Mol. Canc. Ther. 15 (2016) 2107–2118.
[11] (a) L.V. Sequist, S. Gettinger, N.N. Senzer, R.G. Martins, P.A. Jänne, R. Lilenbaum, J.E. Gray, A.J. Iafrate, R. Katayama, N. Hafeez, J. Sweeney, J.R. Walker, C. Fritz, R.W. Ross, D. Grayzel, J.A. Engelman, D.R. Borger, G. Paez, R. Natale, Activity of IPI-504, a novel heat-shock protein 90 inhibitor, in patients with molecularly defined non-small-cell lung cancer, J. Clin. Oncol. 28 (2010) 4953–4960; (b) E.B. Garon, T. Moran, F. Barlesi, L. Gandhi, L.V. Sequist, S.W. Kim, H.J.M. Groen, B. Besse, E.F. Smit, D.W. Kim, M. Akimov, E. Avsar, S. Bailey, E. Felip, Phase II study of the HSP90 inhibitor AUY922 in patients with previously treated, advanced non-small cell lung cancer (NSCLC), J. Clin. Oncol. 30 (2012) 7543; (c) J.W. Goldman, R.N. Raju, G.A. Gordon, I. El-Hariry, F. Teofilivici, V.M. Vukovic, R. Bradley, M.D. Karol, Y. Chen, W. Guo, T. Inoue, L.S. Rosen, A first in human, safety, pharmacokinetics, and clinical activity phase I study of once weekly administration of the Hsp90 inhibitor ganetespib (STA-9090) in patients with solid malignancies, BMC Cancer 13 (2013) 152; (d) D. Mahadevan, D.M. Rensvold, S.E. Kurtin, J.M. Cleary, L. Gandhi, J.F. Lyons, V. Lock, S. Lewis, G. Shapiro, First-in-human phase I study: results of a second-generation non-ansamycin heat shock protein 90 (HSP90) inhibitor AT13387 in refractory solid tumors, J. Clin. Oncol. 30 (2012) 3028; (e) T. Taldone, T. Wang, A. Rodina, N.V.K. Pillarsetty, C.S. Digwal, S. Sharma, P. Yan, S. Joshi, P.P. Pagare, A. Bolaender, G.J. Roboz, M.L. Guzman, G. Chiosis, A chemical biology approach to the chaperome in cancer-HSP90 and beyond, Cold Spring Harb. Perspect Biol. (2019) a034116, https://doi.org/10.1101/cshperspect.a034116.
[12] L. Neckers, P. Workman, Hsp90 molecular chaperone inhibitors: are we there yet? Clin. Cancer Res. 18 (2012) 64–76.
[13] J.M. Patki, S.S. Pawar, Hsp90: chaperone-me-not, Pathol. Oncol. Res. 19 (2013) 631–640.
[14] M. Taddei, S. Ferrini, L. Giannotti, M. Corsi, F. Manetti, G. Giannini, L. Vesci, F.M. Milazzo, D. Alloatti, M.B. Guglielmi, M. Castorina, M.L. Cervoni, M. Barbarino, R. Foderà, V. Carollo, C. Pisano, S. Armaroli, W. Cabri, Synthesis and evaluation of new Hsp90 inhibitors based on a 1,4,5-trisubstituted 1,2,3-triazole scaffold, J. Med. Chem. 57 (57) (2014) 2258–2274.
[15] (a) M.P. Xiong, J.A. Yanez, G.S. Kwon, N.M. Davies, M.L. Forrest, A cremophor-free

formulation for tanespimycin (17-AAG) using PEG-b-PDLLA micelles: characterization and pharmacokinetics in rats, J. Pharm. Sci. 98 (2009) 1577–1586;
(b) M.J. Egorin, E.G. Zuhowski, D.M. Rosen, D.L. Sentz, J.M. Covey, J.L. Eiseman, Plasma pharmcokinetics and tissue distribution, and metabolism of 17-(allylamino)-17-demethoxy-geldanamycin (NSC 330507) in CD2F1 mice, Canc. Chemother. Pharmacol. 47 (2001) 291–302;
(c) D.B. Solit, S.P. Ivy, C. Kopil, R. Sikorski, M.J. Morris, S.F. Slovin, W.K. Kelly, A. DeLaCruz, T. Curley, G. Heller, S. Larson, L. Schwartz, M.J. Egorin, N. Rosen, H.I. Scher, Phase 1 trial of 17- AAG in patients with advanced cancer, Clin. Cancer Res. 13 (2007) 1775–1782;
(d) M.J. Egorin, D.M. Rosen, J.H. Wolff, P.S. Callery, S.M. Musser, J.L. Eiseman, Metabolism of 17-(allylamino)-17- demethoxy-geldanamycin (NSC 330507) by murine and human hepatic preparations, Canc. Res. 58 (1998) 2385–2396.

[16] A.J. Woodhead, H. Angove, M.G. Carr, G. Chessari, M. Congreve, J.E. Coyle, J. Cosme, B. Graham, P.J. Day, R. Downham, L. Fazal, R. Feltell, E. Figueroa, M. Frederickson, J. Lewis, R. McMenamin, C.W. Murray, M.A. O'Brien, L. Parra, S. Patel, T. Phillips, D.C. Rees, S. Rich, D.M. Smith, G. Trewartha, M. Vinkovic, B. Williams, A.J. Woolford, Discovery of (2,4-dihydroxy-5-isopropylphenyl)-[5-(4-methylpiperazin-1-ylmethyl)-1,3-dihydroisoindol-2-yl] methanone (AT13387), a novel inhibitor of the molecular chaperone Hsp90 by fragment based drug design, J. Med. Chem. 53 (2010) 5956–5969.

[17] Y. Wang, J.B. Trepel, L.M. Neckers, G. Giaccone, STA-9090, a small-molecule Hsp90 inhibitor for the potential treatment of cancer, Curr. Opin. Investig. Drugs 11 (2010) 1466–1476.

[18] S.A. Eccles, A. Massey, F.I. Raynaud, S.Y. Sharp, G. Box, M. Valenti, L. Patterson A. de Haven Brandon, S. Gowan, F. Boxall, W. Aherne, M. Rowlands, A. Hayes, V. Martins, F. Urban, K. Boxall, C. Prodromou, L. Pearl, K. James, T.P. Matthews, K.M. Cheung, A. Kalusa, K. Jones, E. McDonald, X. Barril, P.A. Brough, J.E. Cansfield, B. Dymock, M.J. Drysdale, H. Finch, R. Howes, R.E. Hubbard, A. Surgenor, P. Webb, M. Wood, L. Wright, P. Workman, NVP-AUY922: a novel heat shock protein 90 inhibitor active against xenograft tumor growth, angiogenesis, and metastasis, Canc. Res. 68 (2008) 2850–2860.

[19] S. Chatterjee, T.F. Burns, Targeting heat shock proteins in cancer: a promising therapeutic approach, Int. J. Mol. Sci. 18 (2017) E1978.

[20] (a) M.L. Johnson, H.A. Yu, E.M. Hart, B.B. Weitner, A.W. Rademaker, J.D. Patel, M.G. Kris, G.J. Riely, Phase I/II study of HSP90 inhibitor AUY922 and erlotinib for EGFR-mutant lung cancer with acquired resistance to epidermal growth factor receptor tyrosine kinase inhibitors, J. Clin. Oncol. 33 (2015) 1666–1673;
(b) R.N. Rathi, S.R. Ramalingam, Throwing More Cold Water on Heat Shock Protein 90Inhibitors in NSCLC, J. Thor. Onc. 13 (2018) 473–474;
(c) R. Bhat, S.R. Tummalapalli, D.P. Rotella, Progress in the discovery and development of heat shock protein 90 (Hsp90) inhibitors, J. Med. Chem. 21 (2014) 8718–8728.

[21] K. Jhaveri, T. Taldone, S. Modi, G. Chiosis, Advances in the clinical development of heat shock protein 90 (Hsp90) inhibitors in cancers, Biochim. Biophys. Acta 2012 (1823) 742–755.

[22] A. Canella, A.M. Welker, J.Y. Yoo, J. Xu, F.S. Abas, D. Kesanakurti, P. Nagarajan, C.E. Beattie, E.P. Sulman, J. Liu, J. Gumin, F.F. Lang, M.N. Gurcan, B. Kaur, D. Sampath, V.K. Puduvalli, Efficacy of onalespib, a long-acting second-generation HSP90 inhibitor, as a single agent and in combination with temozolomide against malignant gliomas, Clin. Cancer Res. 23 (2017) 6215–6226.

[23] S. Chatterjee, E.H. Huang, I. Christie, B.F. Kurland, T.F. Burns, Acquired resistance to the Hsp90 inhibitor, ganetespib, in KRAS-mutant NSCLC is mediated via reactivation of the ERK-p90RSK-mTOR signaling network, Mol. Cancer Ther. 16 (2017) 793–804.

[24] S. Modi, C. Saura, C. Henderson, N.U. Lin, R. Mahtani, J. Goddard, E. Rodenas, C. Hudis, J. O'Shaughnessy, J.A. Baselga, A multicenter trial evaluating retaspimycin HCL (IPI-504) plus trastuzumab in patients with advanced or metastatic HER2-positive breast cancer, Breast Cancer Res. Treat. 139 (2013) 107–113.

[25] I. El-Hariry, M. Koczywas, V. Vukovic, L. Horn, E. Paschold, R. Salgia, H. West, L.V. Sequist, P. Bonomi, J. Brahmer, L.C. Chen, A. Sandler, C.P. Belani, T. Webb, H. Harper, M. Huberman, S. Ramalingam, K.K. Wong, F. Teofilovici, W. Guo, G.I. Shapiro, A multicenter phase II study of ganetespib monotherapy in patients with genotypically defined advanced non-small cell lung cancer, Clin. Cancer Res. 19 (2013) 3068–3077.

[26] K. Kryeziu, J. Bruun, T.K. Guren, A. Sveen, R.A. Lothe, Combination therapies with HSP90 inhibitors against colorectal cancer, Biochim Biophys. Acta Rev. Cancer. 2019 (1871) 240–247.

[27] K. Nepali, S. Sharma, M. Sharma, P.M.S. Bedi, K.L. Dhar, Rational approaches, design strategies, structure activity relationship and mechanistic insights for anticancer hybrids, Eur. J. Med. Chem. 22 (2014) 422–487.

[28] B. Graham, J. Curry, T. Smyth, L. Fazal, R. Feltell, I. Harada, J. Coyle, B. Williams, M. Reule, H. Angove, D.M. Cross, J. Lyons, N.G. Wallis, N.T. Thompson, The heat shock protein 90 inhibitor, AT13387, displays a long duration of action in vitro and in vivo in non-small cell lung cancer, Canc. Sci. 103 (2012) 522–527.

[29] D.A. Proia, R.C. Bates, Ganetespib and HSP90: translating preclinical hypotheses into clinical promise, Canc. Res. 74 (2014) 1294–1300.

[30] R. Musiol, An overview of quinoline as a privileged scaffold in cancer drug discovery, Expert Opin Drug Discov. 12 (2017) 583–597.

[31] T. Ganesh, J. Min, P. Thepchatri, Y. Du, L. Li, L. Lewis, L. Wilson, H. Fu, G. Chiosis, R. Dingledine, D. Liotta, J.P. Snyder, A. Sun, Discovery of aminoquinolines as a new class of potent inhibitors of heat shock protein 90 (Hsp90): synthesis, biology and molecular modeling, Bioorg. Med. Chem. 16 (2008) 6903–6910.

[32] S.O. Malayeri, K. Abnous, A. Arab, M. Akaberi, S. Mehri, A. Zarghi, R. Ghodsi, Design, synthesis and biological evaluation of 7-(aryl)-2,3-dihydro- [1,4]dioxino [2,3-g]quinoline derivatives as potential Hsp90 inhibitors and anticancer agents, Bioorg. Med. Chem. 25 (2017) 1294–1302.

[33] K. Nepali, S. Kumar, H.L. Huang, F.C. Kuo, C.H. Lee, C.C. Kuo, T.K. Yeh, Y.H. Li, J.Y. Chang, J.P. Liou, H.Y. Lee, 2-Aroylquinoline-5,8-diones as potent anticancer agents displaying tubulin and heat shock protein 90 (HSP90) inhibition, Org. Biomol. Chem. 14 (2016) 716–723.

[34] (a) M.J. Lai, J.Y. Chang, H.Y. Lee, C.C. Kuo, M.H. Lin, H.P. Hsieh, C.Y. Chang, J.S. Wu, S.Y. Wu, K.S. Shey, J.P. Liou, Synthesis and biological evaluation of 1-(4'-Indolyl and 6'-Quinolinyl) indoles as a new class of potent anticancer agents, Eur. J. Med. Chem. 46 (2011) 3623–3629;
(b) Y.M. Liu, H.Y. Lee, C.H. Chen, C.H. Lee, L.T. Wang, S.L. Pan, M.J. Lai, T.K. Yeh, J.P. Liou, 1-Arylsulfonyl-5-(N-hydroxyacrylamide)tetrahydroquinolines as potent histone deacetylase inhibitors suppressing the growth of prostate cancer cells, Eur. J. Med. Chem. 89 (2015) 320–330.

[35] H.Y. Lee, K. Nepali, F.I. Huang, C.Y. Chang, M.J. Lai, Y.H. Li, H.L. Huang, C.R. Yang, J.P. Liou, (N-Hydroxycarbonylbenylamino) quinolines as selective histone deacetylase 6 inhibitors suppress growth of multiple myeloma in vitro and in vivo, J. Med. Chem. 61(2018) 905–917.

[36] H.M. Berman, J. Westbrook, Z. Feng, G. Gilliland, T.N. Bhat, H. Weissig, I.N. Shindyalov, P.E. Bourne, The protein data bank, Nucleic Acids Res. 28 (2000) 235–242.

[37] LeadIT, B. < http://www.biosolveit.de/LeadIT > (accessed 12th January, 2011).